Separation and Purification Technology 295 (2022) 121347

Contents lists available at ScienceDirect

Separation and Purification Technology

journal homepage: www.elsevier.com/locate/seppur

Co@CoO encapsulated with N-doped carbon nanotubes activated peroxymonosulfate for efficient purification of organic wastewater

Chuanyi Xu [a,d,1], Qingyou Liu [e,1], Meng Wei [a], Shihui Guo [a], Yueping Fang [a,d], Zhuobiao Ni [b,d,*], Xixian Yang [c,*], Shengsen Zhang [a,d,*], Rongliang Qiu [b,d]

[a] Key Laboratory for Biobased Materials and Energy of Ministry of Education, College of Materials and Energy, South China Agricultural University, Guangzhou, 510642, China
[b] Guangdong Provincial Key Laboratory of Agricultural & Rural Pollution Abatement and Environmental Safety, College of Natural Resources and Environment, South China Agricultural University, Guangzhou 510642, China
[c] Institute of Biomass Engineering, Key Laboratory of Energy Plants Resource and Utilization, Ministry of Agriculture and Rural Affairs, Guangdong Engineering Technology Research Center of Agricultural and Forestry Biomass, South China Agricultural University, Guangzhou, 510642, China
[d] Guangdong Laboratory for Lingnan Modern Agriculture, Guangzhou 510642, China
[e] Key Laboratory of High-temperature and High-pressure Study of the Earth's Interior, Institute of Geochemistry, Chinese Academy of Sciences, Guiyang, 550081, China

ARTICLE INFO

Keywords:
Surface oxidized nano-cobalt
N-doped carbon nanotubes
Peroxymonosulfate
Organic wastewater
Advanced oxidation
Intermediate analysis

ABSTRACT

Catalytic activation of peroxymonosulfate (PMS) for purifying organic wastewater has been widely studied. However, the activation mechanism either by free radicals or non-radicals alone is not satisfactory efficiency. In this work, a novel advanced oxidation system based on surface oxidized metallic cobalt nanoparticles (Co@CoO) encapsulated with N-doped carbon nanotubes (NCT), i.e., CCN, activated peroxymonosulfate (PMS) was designed. The CCN-PMS system showed excellent performance in the degradation for a wide range of organic pollutants, including antibiotics, dyes, and phenols. The degradation rate of 100 mL 80 mg·L^{-1} tetracycline hydrochloride (TC) in the system (10 mg CCN + 0.5 mM PMS) reached 92% within 30 min. The mechanism analysis of the CCN activation of PMS reveals that the NCT mainly provided the active sites for non-radical formation, while the Co@CoO mainly provided the active sites for radical formation. In addition, the NCT could not only effectively reduce the leaching of Co^{x+}, but also play a synergistic role with Co@CoO in the degradation of organic pollutants. This work provides new insight into the mechanism of PMS activation by carbon-based catalysts for the efficient purification of organic wastewater.

1. Introduction

Advanced oxidation processes (AOPs) based on peroxymonosulfate (PMS) is considered as a promising method for purifying organic wastewater [1]. The active components are mainly hydroxyl radicals (•OH) and sulfate radicals ($SO_4^{\bullet-}$) generated during the activation of persulfate [2]. The activation of PMS commonly includes catalytic techniques and energy-driven approaches. The former usually uses catalysts containing transition metal ions [3] and base [4], while the latter requires energy usually from heating [5], UV irradiation [6] or ultrasonic energy-driven [7], etc. The energy-driven activation has some inherently problems including high cost and complicated operation equipment, leading to difficulty in achieving large-scale practical application. On the other hand, the catalytic activation of PMS has been widely investigated due to its simple operation, low cost and high efficiency.

Previous researches have shown that •OH and $SO_4^{\bullet-}$ can be generated by the catalytic activation of PMS with various transition metal ions, including Co^{2+}, Mn^{2+}, Fe^{2+} and so on [3]. Both •OH and $SO_4^{\bullet-}$ are non-selective and strong oxidizers with a redox potential of 1.8 ~ 2.7 eV and 2.5 ~ 3.1 eV, respectively, allowing them to oxidize more refractory pollutants [8,9]. Among the transition metal ions, Co^{2+} has been proved to be one of the most effective homogeneous catalysts for activating PMS [10]. However, a fatal drawback of the Co^{2+} activator lies in the poor stability and potential secondary pollution for water bodies as it is easily soluble in water and difficult to be separated from water [11]. Therefore,

* Corresponding authors.
E-mail addresses: nizhuobiao@scau.edu.cn (Z. Ni), yangxixian@yeah.net (X. Yang), zhangss@scau.edu.cn (S. Zhang).
[1] These authors made equal contributions to this work.

https://doi.org/10.1016/j.seppur.2022.121347
Received 6 April 2022; Received in revised form 8 May 2022; Accepted 22 May 2022
Available online 25 May 2022

the preparation of efficient and insoluble cobalt-based activators has become a desirable direction for researchers [12]. Pioneering studies have shown that carbon material is metal-free with a high specific surface area, and can serve as a functional carrier of Co^{2+} activator [13]. The superiority of Co/C-based materials as the activator of PMS is attributed to the fact that the carbon materials not only reduce the leaching of Co^{2+} by dispersing it into the carbonaceous material, but also improve their activation performance through the synergistic effect of Co^{2+} and carbon materials. For example, Shukla et al. applied a multiphase cobalt-based catalyst based on activated carbon impregnated with Co^{2+} for deep phenol oxidation, resulting in efficient activation of PMS with reasonable stability [14]. Wang et al. designed a PMS activator of core–shell Co@C nanoparticles with N and S doped porous carbons (Co-N-S-PCs) that showed high efficiency of oxidative decomposition of p-hydroxybenzoic acid and phenol [15].

Besides carrying the Co^{2+} activator for PMS activation, carbon material itself can also act as the activator for PMS, mainly by generating large amounts of non-radicals to degrade organic pollutants [16,17]. Non-radical oxidation processes exhibit moderate redox potentials, allowing the non-radicals to resist interference from inorganic ions and background organic matter [17]. Among carbonaceous materials, carbon nanotubes (CNTs) are preferred materials for activating PMS to degrade organic pollutants due to their rich porosity and excellent electronic conductivity [18]. However, their catalytic performance is hindered by the inertness of the carbon element [19]. Modification by doping with N, S, B, P and other heteroatoms can modulate the electronic states and active sites within the matrix of carbon materials, and thus improve their activation properties [20]. For example, N atoms can effectively promote the electron transfer of adjacent carbon and increase the charge density of carbon atoms, thus increasing the adsorption energy of carbon atoms with PMS molecules [21]. Meanwhile, the N doping leads to the formation of defects on the carbon skeleton, providing certain active sites for the reaction [22]. Although these improvements can enhance the activation performance of N-doped carbon nanotubes to certain extent, the mechanism of producing non-radicals to degrade pollutants leads to lower catalytic performance after all than that ofradicals. Thus, further optimizations are required.

To sum up, the efficiency of PMS activation for organic wastewater degradation by either free radicals or non-radicals alone was not yet satisfactory. To this end, we designed a novel system which provides the coexistence reaction of radicals and non-radicals from the activation of transition metal ions and carbon materials, respectively, to achieve superior catalytic performance. This work is the first to apply surface oxidized metallic cobalt nanoparticles (Co@CoO) encapsulated with N-doped carbon nanotubes (NCT) material, i.e., CCN, to activate the PMS for purification of organic wastewater. The degradation performance of such a CCN-PMS system on tetracycline hydrochloride (TC) as the representative of the organic pollutant was comprehensively investigated. The various effects of Co salt dosages, PMS dosages, pollutant concentration, organic wastewater pH values, the existence of different anions and humic acids in the wastewater on the degradation performance were explored. Meanwhile, the recyclability and practicability of the catalyst was also tested. Via quenching experiment, electron paramagnetic resonance spectra, electrochemical performance characterization, and LC-Q-TOF analysis on the intermediates of TC conversion, the activation mechanism of CCN on PMS as well as possible degradation pathways of TC were derived.

2. Materials and methods

2.1. Reagents and materials

All chemical reagents were purchased from Sigma-Aldrich Trading Co., LTD. They are all AR reagent grade and can be used as initial conditions without further purification. Deionized water was used for all solutions. The domestic filtrate wastewater comes from Guangzhou, China, and the raw leachate contains approximately 8000 $mg{\cdot}L^{-1}$ COD and 1600 $mg{\cdot}L^{-1}$ ammonia nitrogen. In our laboratory, we pretreat this leachate with a Fenton oxidation process. The effluent still contains approximately 1000 $mg{\cdot}L^{-1}$ COD and 700 $mg{\cdot}L^{-1}$ ammonia nitrogen.

2.2. Synthesis of catalyst

2.2.1. Synthesis of graphitic carbon nitride (g-C_3N_4)

The carbon nitride (g-C_3N_4) was synthesized by a slight modification of the previous method [23]. 6 g of urea was placed in a crucible in a muffle furnace and calcined in air at 550 °C for 2 h, and then allowed to cool naturally to room temperature. The sample was taken out and ground in a mortar for 30 min to obtain g-C_3N_4.

2.2.2. Synthesis of nanomaterials Co@CoO/NCT (CCN)

0.6 g of pluronic was placed in a beaker with the addition of 60 mL of deionized water, and stirred with a magnetic stirrer until the solution became colorless and transparent. Afterwards, 0.4 g of the above g-C_3N_4 was added to the mixed solution and sonicated for 3.5 h for complete dispersion the mixed solution completely, followed by dropwise addition of 0.2 $mol{\cdot}L^{-1}$ $Co(NO_3)_2$ stock to the mixed solution and continuous stirring of 12 h. Next, the mixture was stirred and dried in the beaker was placed in an oil bath (90 °C). Then, the sample was placed in an oven at 150 °C for 2 h to obtain the precursor. Subsequently, the sample was heated at a heating rate of 2 $°C{\cdot}min^{-1}$ from room temperature to 550 °C and kept for 2 h followed by another temperature rising rate of 2 $°C{\cdot}min^{-1}$ to 800 °C and kept for another 2 h under nitrogen protection. Finally, a fluffy black sample was obtained after cooling in the tube furnace. Five samples were obtained by varying the volume of the added $Co(NO_3)_2$ solution, namely 0.0 mL, 1.0 mL, 2.0 mL, 3.0 mL and 4.0 mL, and denoted as NC, CCN1, CCN2, CCN3 and CCN4, respectively.

2.3. Material characterization

The powder X-ray diffraction (XRD) patterns were performed on an Ultima IV X-ray diffractometer (Riken, Japan) at 40 kV and 40 mA with a Cu Kα1 (λ = 1.54056 A) radiation source. Through testing the Brunauer–Emmett–Teller (BET) specific surface areas (SBET, Quantachrome, USA) of the samples, the pore size distributions were obtained, of which the influence on the experimental conditions were also explored. The scanning electron microscopy (SEM) of the sample was characterized by Merlin (Carl Zeiss AG, Germany) at an accelerating voltage of 5 kV. The high-resolution transmission electron microscopy (HRTEM) was performed to observe the surface morphology and lattice striations of the sample at H-800 (Hitachi, Japan) at an accelerating voltage of 200 kV. The BET specific surface area was obtained at Gemini-2390 (Mack Instruments, USA). X-ray photoelectron spectroscopy (XPS) was analyzed at Escalab 250xi (thermometer fisher, USA) under the monochromatic Al Kα X-ray source (300 W, 5 mA, 15 kV). The functional groups of carbon materials were determined by Flourier transform infrared (FTIR) spectrometry (Nexus 670, USA). The electron paramagnetic resonance (EPR) spectra were recorded using a JES FA200 (JEOL, Japan) (Text S1 in Supplementary Material). Linear sweeping voltammetry (LSV) and impedance (EIS) were tested using an electrochemical workstation (CHI-650e) Shanghai Chenhua Instruments Co., LTD (Text S2 in Supplementary Material). The concentration of aromatic contaminants was tested using High Performance Liquid Chromatography Agilent 1100 Series (Agilent Technologies Co., Ltd.) and the degradation products of aromatic pollutants were tested using LC-Q-TOF (Uplc1290-6540B Agilent Technologies Co., Ltd.)(Text S3 in Supplementary Material). The total organic carbon (TOC) was measured by TOC analysis meter (Vario TOC, Elementar). The Chemical Oxygen Demand (COD) of wastewater was measured by rapid digestion-spectrophotometric method. The ammonia nitrogen content was tested by Nessler's reagent spectrophotometry. The concentration of organic dyes was determined by UV spectrophotometer (Guangzhou Shuopu

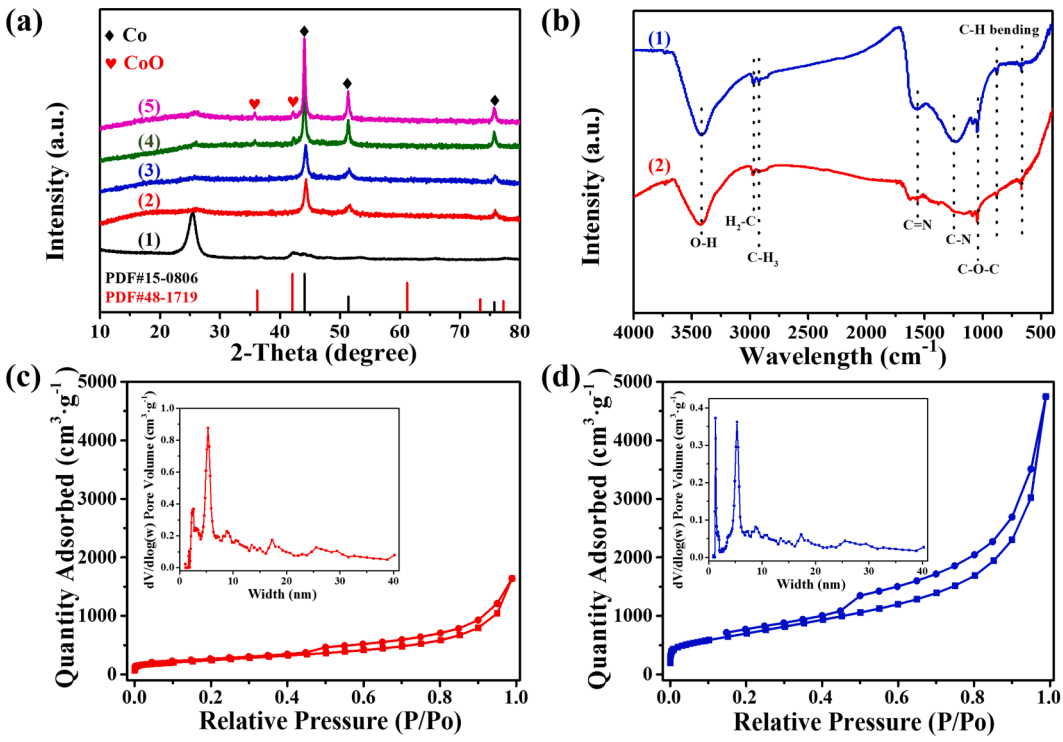

Fig. 1. (a) XRD of CCN prepared with (1) 0 mL, (2) 1.0 mL, (3) 2.0 mL, (4) 3.0 mL, (5) 4.0 mL of the added $Co(NO_3)_2$ solution; (b) FTIR of (1) NC and (2) CCN3; N_2 adsorption–desorption isotherms and pore size distribution maps of (c) NC and (d) CCN3.

Biotechnology Co., Ltd.).

2.4. Catalytic activity measurement

10 mg of catalyst was added to 100 mL of TC solution (50 ~ 100 mg·L^{-1}) and stirred continuously for 30 min under the dark environment to reach adsorption equilibrium. Then, a certain amount of PMS (0.25 ~ 0.75 mM) was added to trigger the degradation of the contaminants. 1.0 mL of liquid sample was taken periodically and then filtered through a 0.22 μm nylon syringe filter membrane. The concentration of TC was determined by HPLC equipped with an Agilent Eclipse XDB-C18 column (5 μm, 4.6 mm × 250 mm). The mobile phase was a mixture of methanol, acetonitrile and 0.01 mol·L^{-1} oxalic acid aqueous solution in the ratio of 15:15:70 (v/v/v %) with a flow rate of 1.0 mL·min^{-1}, the detection wavelength set to 280 nm and the column temperature set to 33 °C.

To determine the reusability of CCN in the advanced oxidation process, cyclic degradation experiments of TC were performed. The CCN collected after each cycle was washed ultrasonically using deionized water and dried under vacuum at 60 °C, and later on was applied for the next cycle of the experiment. To determine the practicality of CCN in the advanced oxidation process, the performance of this system was tested on practical wastewater. 10 mg of catalyst was added to 100 mL of practical landfill leachate (pre-treated) and 0.5 mM PMS was added to trigger the reduction of the COD and ammonia nitrogen.

3. Results and discussion

3.1. Structure and characterization

The XRD results of the NC or CCN catalysts with different volumes of the added 0.2 mol·L^{-1} $Co(NO_3)_2$ solution are shown in Fig. 1a. The diffraction peaks at 44.21°, 51.52° and 75.85° (JCPDS #no. 15–0806) corresponded to the (1 1 1), (2 0 0) and (2 2 0) different crystallographic planes of metallic Co, respectively. The intensity of the diffraction peak of Co increased with the increase of Co sources. It is noteworthy that two weak peaks corresponding to (1 1 1) and (2 0 0) different crystal planes of CoO appeared at 36.49° and 42.38° (JCPDSF #no. 48–1719). This might be due to the partial oxidation of the surface of metallic Co, indicating that the sample contains a large amount of metallic Co nanoparticles and a small amount of CoO nanoparticles. Besides, one graphitized carbon peak appeared around 26.10°, which can be attributed to the fact that the added Co can act as a catalyst to generate graphitized carbon in the presence of carbon source conditions [23].

Via FTIR spectra of NC and CCN3 (Fig. 1b), abundant functional groups that are essential for activating PMS [24], could be observed on the sample surface. The peaks at 3420 cm^{-1}, 2970 cm^{-1}, 2920 cm^{-1}, 900 cm^{-1} and 650 cm^{-1} could be classified as –OH, C—H_2 or C—H_3, C—H bending for aromatic out of plane deformation, respectively. The C═N bond at 1580 cm^{-1} and the C—O—C bond at 1052 cm^{-1} did not change significantly after Co doping [25]. However, the peaks of CCN3 at 1267 ~ 1274 cm^{-1} (C—N bond) were significantly less intense than those of the NC sample. A plausible explanation could be that the C—N bond was disrupted and a new chemical bond after the doping of Co [26]. In addition, other oxygen-containing functional groups, such as C═O groups were identified on the surface of CCN. They will be beneficial to the PMS activation and will further promote the non-radical catalytic pathway [27].

Specific surface area and pore size distribution of catalysts are important factors for catalytic activity. The specific surface areas of CCN3 and NC samples were measured by the Brunauer Emmett Teller (BET) method. Fig. 1c–d shows the N_2 adsorption–desorption equilibrium results of different samples in agreement with those of carbon nanotubes. Table S1 shows that the specific surface of the N-doped carbon nanotubes containing Co was 1248.9 $m^2·g^{-1}$, while the N-doped sample without adding Co was only 481.4 $m^2·g^{-1}$. The reason is that the carbon material of NC did not form nanotubes in the absence of the Co source [28], and its specific surface area was much smaller than that of CCN3. The pore distribution is shown in the inset of Fig. 1c–d. The distribution of pore size larger than 5 nm appeared rather consistent in both NC and CCN3. In terms of micropores, especially around 1.5 nm, CCN3 presented the significantly larger distribution compared to NC.

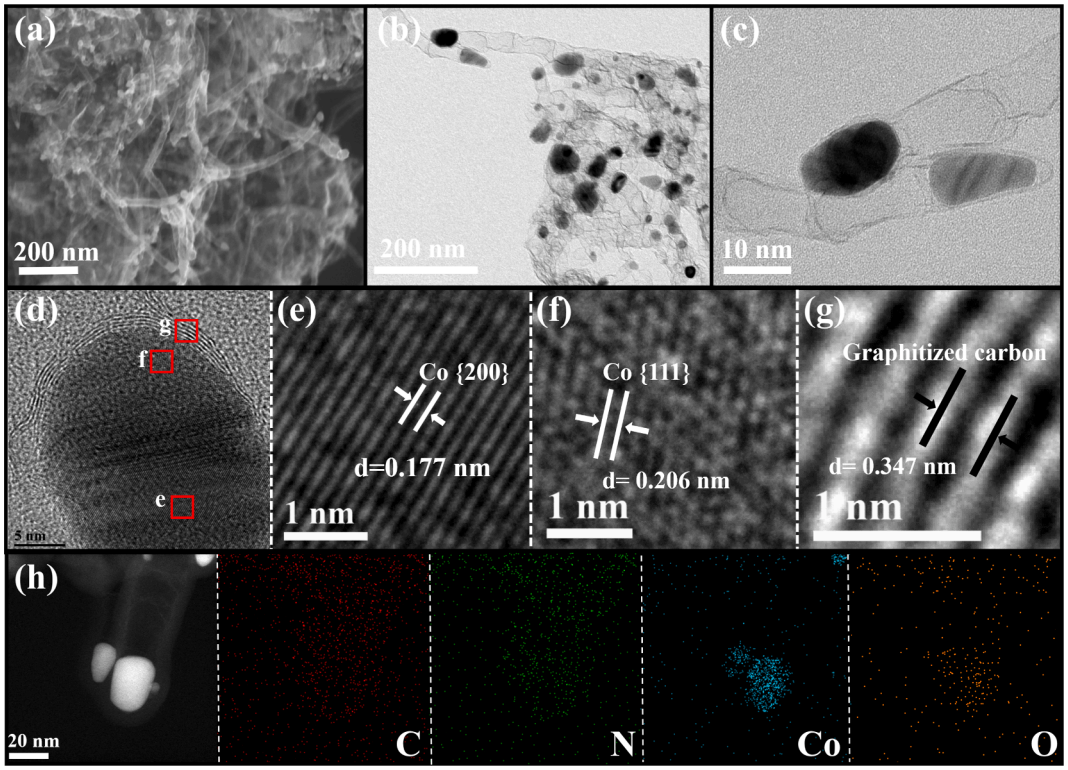

Fig. 2. SEM (a), TEM (b, c), HRTEM (d–g) and TEM-EDX element mapping (h) of CCN3.

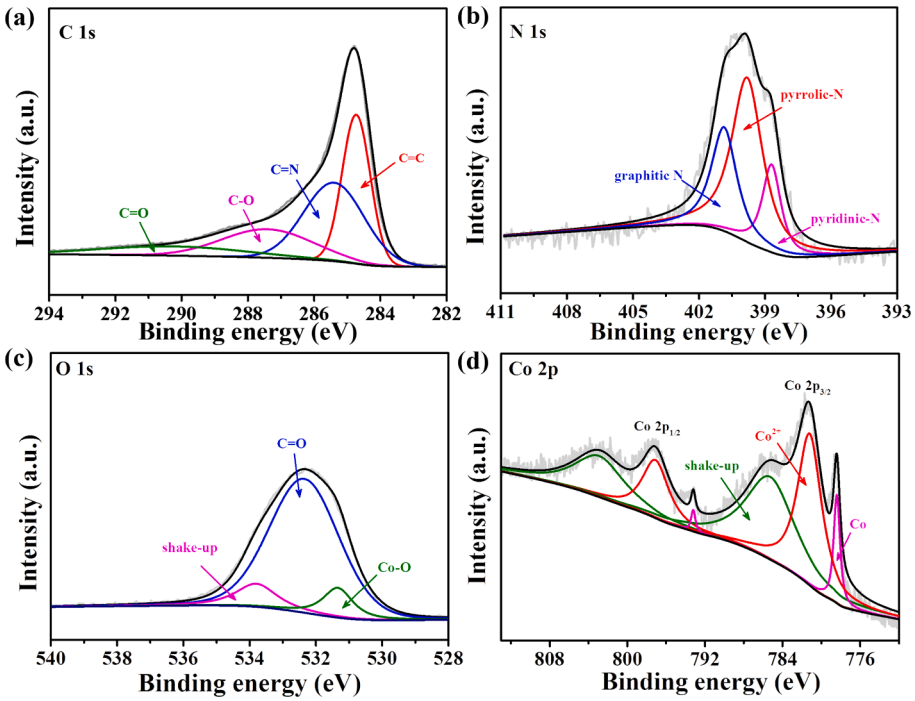

Fig. 3. XPS spectra of 3-CCN: (a) C1s, (b) N 1 s, (c) O 1 s, (d) Co 2p.

The large specific surface area of CCN3 and the presence of plenty microspores and mesoporous could provide more catalyst active sites and improve the performance of activated PMS.

The SEM image reveals larger amounts of nanotubes in the CCN3 sample (Fig. 2a). Some particles with a size of ca. 20 nm (white dots) were encapsulated within the nanotubes, and most of which were located at the top of the nanotubes with tight-binding. In contrast, the NC sample did not form nanotubes (Figure S1). It can be inferred that the Co source plays an important role in the generation of carbon nanotubes by acting as a catalyst [28], and the movement of cobalt particles during annealing process facilitating the formation of carbon nanotubes [29]. The TEM images of CCN3 display that the sample had well-shaped bamboo-like nanotubes, in which the metal particles were well encapsulated (Fig. 2b–c). The HRTEM images of CCN3 (Fig. 2d-g) show that

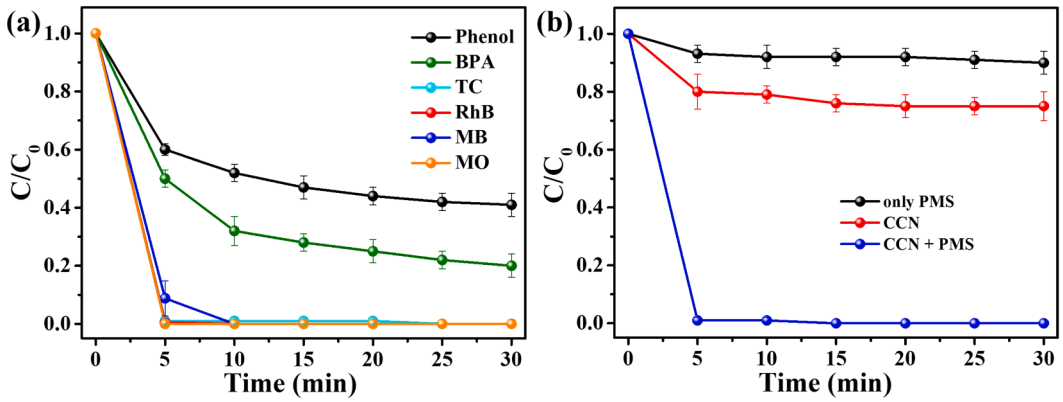

Fig. 4. (a) The CCN3-PMS system for the degradation of various aromatic organic pollutants; (b) The removal rate of TC by CCN3, PMS and CCN3-PMS system. ($[CCN3]_0$ = 0.1 g·L^{-1}, $[pollutants]_0$ = 50 mg·L^{-1}, $[PMS]_0$ = 0.75 mM, pH = 3.4).

the lattice stripes with a spacing of 0.177 nm and 0.206 nm corresponding to the (200) and (111) planes of nano-Co, respectively. The lattice spacing of 0.347 nm between the particle edge and surface layer can be attributed to the graphitic carbon layer. The distribution of C, N, Co and O in CCN3 was analyzed by TEM-EDX element mapping (Fig. 2h), illustrating that the C and N elements were uniformly distributed on the nanotubes, whereas the Co and O elements were distributed at the top of the nanotubes.

To clarify the chemical bonding and valence states of the surface elements of CCN, XPS analysis on the CCN3 sample was performed. The XPS survey spectra of the sample before and after reaction are shown in Figure S2a. The detected C, N, O, and Co elements originated from the Co@CoO and N-doped carbon nanotubes. The XPS spectrum of C 1 s (Fig. 3a) can be fitted to four typical peaks at 284.7 eV, 285.6 eV, 286.8 eV and 288.6 eV corresponding to C—C, C═N, C—O—C and C═O [8], respectively. This indicates that N was successfully doped into carbon nanotubes, agreeing with the result from the FTIR. The N 1 s spectrum of the CCN3 is fitted to three peaks (Fig. 3b) corresponding to three types of N functions, namely pyrimidine nitrogen (398.7 eV), pyrrole nitrogen (399.8 eV), and graphite nitrogen (400.8 eV) (corresponding to C═N) [16]. The O 1 s XPS spectrum peaks (Fig. 3c) are deconvoluted into two peaks at 531.3 eV and 532.3 eV corresponding to Co—O [30], and carboxylate (O—C═O) [31], respectively. Moreover, in the Co 2p XPS spectra before the reaction (Fig. 3d), the fitted peaks at 781.2 eV and 797.1 eV were consistent with the signals of Co $2p_{3/2}$ and $Co2p_{1/2}$ of Co^{2+}, while the fitted peaks at 778.5 eV and 793.2 eV were stemming from metallic Co [32]. In addition, the intensity of the peak of Co^{2+} was significantly stronger than that of metallic Co, implying that the outer layer of CCN3 nanoparticles was CoO, as the XPS technology characterizes the valence state mainly of the surface of the material. Combining with the result from the HRTEM of the CCN3 showing only the lattice of metallic Co but not CoO, it is confirmed that the metallic Co was covered by a thin layer of CoO on the outside.

In summary, the results from XRD, FTIR, SEM, TEM, and XPS characterization proved that surface oxidized metallic Co nanoparticles encapsulated with N-doped carbon nanotubes were successfully achieved.

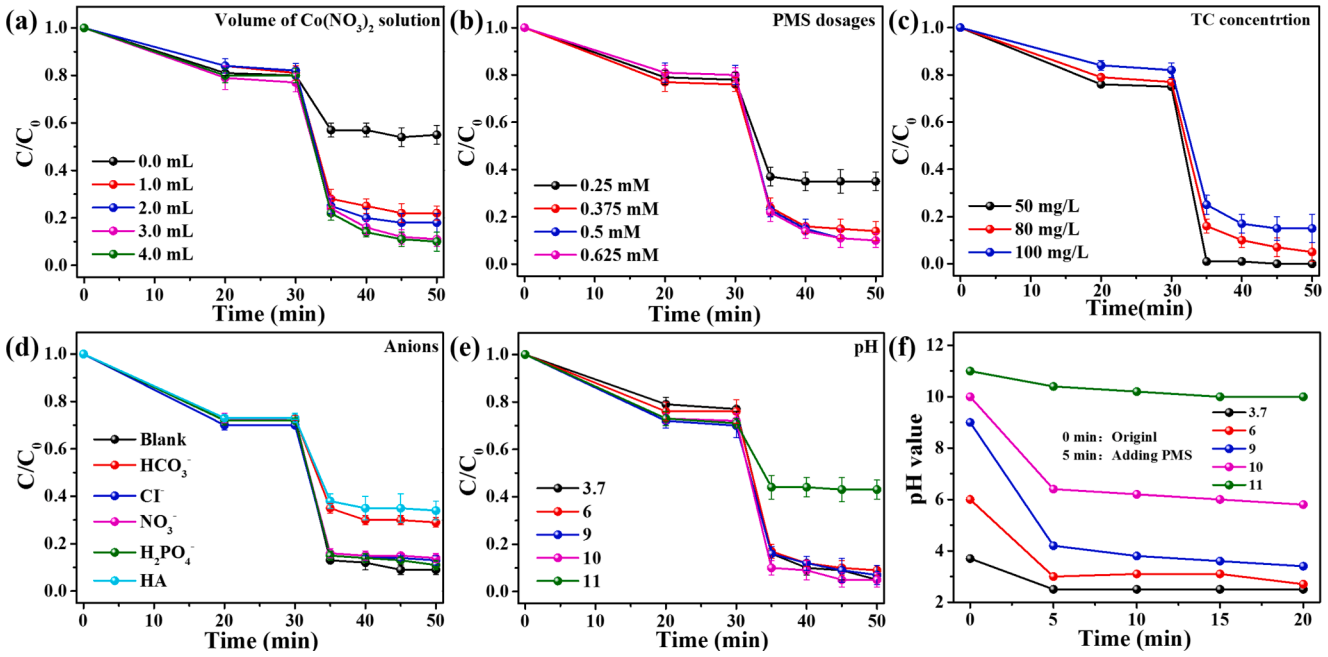

Fig. 5. (a) Effect of different factors on the efficiency of degradation of TC (80 mg·L^{-1}) in the CCN3-PMS system: (a) amount of $Co(NO_3)_2$ precursor, (b) concentration of PMS, (c) concentration of TC, (d) various typical anions and humic acids (the concentration of typical anions was 0.25 mM), (e) different pH values; (f) pH changes during the degradation of TC. (Optimal conditions: 80 mg·L^{-1} TC, 0.5 mM PMS, 3 mL $Co(NO_3)_2$ solution were used to prepare CCN3, and the initial pH was 3.7.).

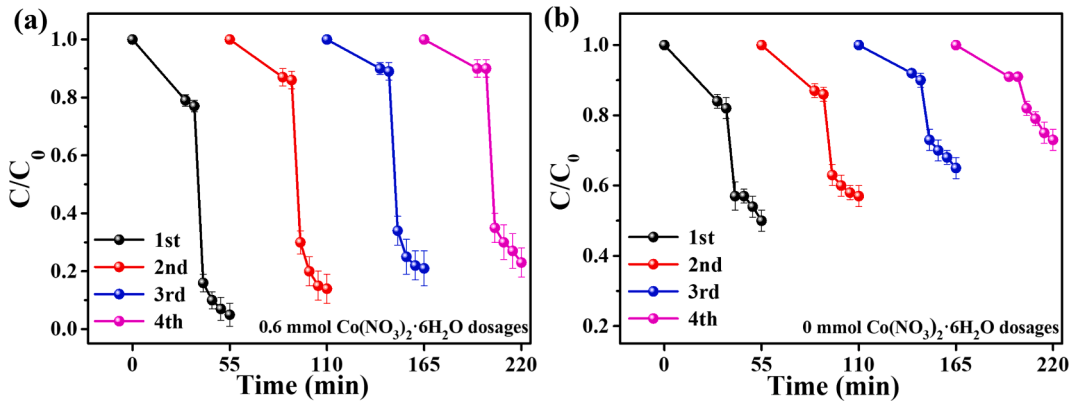

Fig. 6. The reusability of CCN (a) and NC (b) in the PMS system for the degradation of TC.

3.2. Catalytic activity of NC and CCN catalysts

The degradation of various aromatic organic pollutants antibiotics (TC), dyes including methyl orange (MO), methyl blue (MB) and rhodamine (RhB), and phenols including bisphenol A (BPA) and phenol (Phenol) in the CCN3-PMS system were investigated. As shown in Fig. 4a, the CCN3-PMS system exhibited efficient degradation in those mentioned above aromatic organic pollutants. As a representative antibiotic, TC was selected to evaluate the pollutant removal performance of the CCN3-PMS system. First, such the system presented good adsorption performance (Fig. 4b). The adsorption equilibrium was achieved within 30 min, with an adsorption capacity for 50 $mg{\cdot}L^{-1}$ TC (100 mL) reaching over 20%. Second, the large surface area (1248.9 $m^2{\cdot}g^{-1}$) allows TC molecules to diffuse from the solution into the pores of the catalyst, facilitating sufficient contact between the catalyst and TC inside the carbon matrix [33]. With the addition of PMS, the removal rate of TC by the CCN3-PMS system increased to 100% within 5 min. Such efficiency remarkably outperformed the scenario of PMS only, which experienced a poor removal rate of 6.4%, under the same experimental conditions. These results demonstrate that the CCN3 sample has not only good adsorption capacity for TC, but also possesses excellent activation performance for PMS.

Various factors affecting the TC removal efficiency in the CCN-PMS system were investigated, including the amount of Co source, i.e. the volume of the added $Co(NO_3)_2$ solution, amount of PMS, TC concentration, pH, different anions and humic acids (HA) in the TC wastewater (Fig. 5). In general, the degradation rate of TC increased with the increase of $Co(NO_3)_2$ solution from 0.0 ~ 4.0 mL (Fig. 5a). However, the TC degradation rate did not improve any further when the added volume was above 3.0 mL. Therefore, 3.0 mL of $Co(NO_3)_2$ solution was chosen as the optimal Co source addition amount, i.e., CCN3. Notably, the catalyst NC also exhibited certain degradation efficiency for TC when no Co salt was added, indicating that the N-doped carbon could activate PMS [16,34]. The reaction rate constants obtained by fitting the data as shown in Figure S3, showed that the K value increased from 0.015 to 0.094 when Co was added, indicating that the activation of PMS was facilitated by the addition of Co. In order to investigate the optimal conditions for the CCN-PMS system to purify TC wastewater and explore the related reaction mechanism, the CCN3 sample was used for the subsequent experiments.

Next, the effects of different amounts of PMS were discussed as the amount of PMS plays a crucial role in the oxidation reaction of TC in the system. Higher PMS dosage generally resulted in more effective TC degradation (Fig. 5b). The treatment with 0.375 mM PMS already exhibited the best removal performance with a degradation rate exceeding 91%. As the removal could not improve further with a PMS concentration above 0.5 mM, thus which was selected as the optimal dosage of PMS. The effect of TC concentration on the degradation process was revealed to be adverse during the experiments (Fig. 5c). The degradation rate decreased gradually with the increases of TC concentration, indicating that more active substances are needed to react to degrade the pollutants of higher concentration in the system.

As inorganic anions and HA in the actual water body can affect the degradation of organic pollutants in the PMS-based oxidation system [35], their effects on the TC degradation in the CCN3-PMS system were investigated. Previous research demonstrated that some anions like Cl^-, NO_3^-, $H_2PO_4^-$ and HCO_3^- can react with free radicals ($SO_4^{\bullet-}$ and •OH) to form weaker free radicals, resulting in lower degradation efficiency [33]. However, the experiments of the CCN3-PMS system show strong resistance to negative interferences, as no significant inhibition on the TC degradation by Cl^-, NO_3^-, and $H_2PO_4^-$ was observed (Fig. 5d). This is due to the fact that non-radical AOPs can overcome the inhibitory effect of anions and plays an important role in PMS activation, reflecting that the CCN3-PMS system is robust to anions interference. The HCO_3^- also had an inhibitory effect on the CCN3-PMS system because HCO_3^- is a strong bursting agent for $SO_4^{\bullet-}$ and •OH, which alters the pH of the system during the degradation process [36]. These results suggest that the $SO_4^{\bullet-}$ and •OH were the main active species in the CCN3-PMS system for the degradation of TC. Fig. 5d displays that TC degradation was inhibited in CCN3-PMS after the addition of HA. Although natural organic matter (such as HA) is capable of quenching $SO_4^{\bullet-}$ and •OH radicals and binding active sites of metals [37], 70.1% of the TC could still be degraded within 20 min with the addition of PMS. This indicates the presence of some unknown reactive substances other than radicals (such as non-radicals) in the CCN3-PMS system, which were responsible for the TC degradation. Finally, the effect of pH on TC degradation was investigated. The degradation efficiency changed rather slightly in the treatments with a pH range of 3.7 ~ 10 due to the good catalytic stability of CCN3 (Fig. 5e). These treatments also experienced a sharp drop of pH within the first 5 min (Fig. 5f). However, the oxidation capacity in condition with initial pH of 11 decreased significantly during the treatment, which showed no obvious change in pH at the end of the experiment. Under such conditions, nevertheless, 59.6% of TC was still removed, proving that the NC in addition to Co did play an important role in this system. Under acidic conditions, a more positive charge on the catalyst surface can be achieved, which is conducive to attracting PMS. The active site on the surface of the N-doped carbon catalyst is beneficial for reacting with PMS under lower pH conditions [33]. Therefore, within the initial pH range of 3.7 ~ 10, the oxidation ability of the CCN3-PMS system was almost unchanged. However, when the initial pH was 11, the pH of the solution was kept at 10.2 after PMS was added, and the degradation efficiency of TC was significantly reduced. Under alkaline conditions (pH = 10.2), Co^{2+} was complexed and deposited, thus reducing the activation of the PMS [8].

In practical industrial applications, the catalyst lifetime is an important factor in evaluating its performance. The reusability of NC

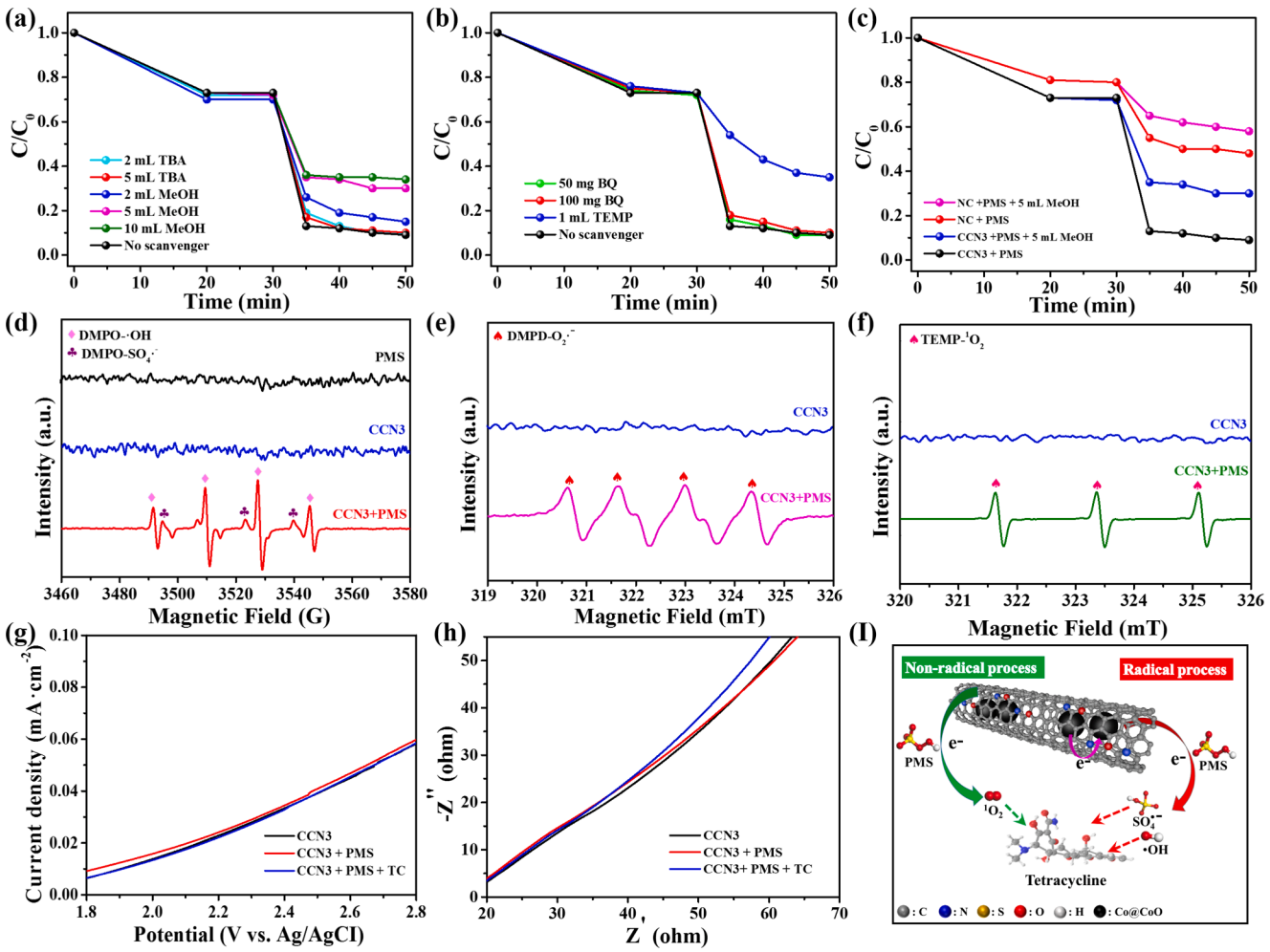

Fig. 7. TC degradation performance of CCN3-PMS system with different scavengers (a) TBA and MeOH, (b) BQ and TEMP, (c, d) EPR test of $SO_4^{\bullet-}$, •OH and $\bullet O_2^-$, (e) CCN3 and NC with and without scavengers (MeOH); (f) EPR test of $^1O_2$; (g) LSV and (h) EIS curves obtained under different conditions ([catalyst]$_0$ = 0.1 g·L^{-1}, [TC] 0 = 80 mg·L^{-1}, [PMS]$_0$ = 0.5 mM, the electrolyte was 0.05 M Na_2SO_4 solution); (I) Schematic diagram of the degradation mechanism of TC in the CCN3-PMS system.

and CCN3 were compared in this experiment. Fig. 6 exhibits that the degradation activity and stability of the CCN3 catalyst were significantly better than that of NC. In the CCN3-PMS system, though the catalyst activity slightly decreased with the increase of cycles, the degradation rate of TC remained ca. 80%, and the removal of TOC remained ca. 72% (Figure S4) even after 4 cycles. In addition, the XRD and SEM characterization of the reacted CCN3 sample (Figures S5 and S6) confirmed that its crystal structure remained unchanged. The metal nanoparticles were still tightly wrapped by carbon nanotubes, preventing the dissolution of cobalt ions (Co^{x+}). By comparing with other carbon-based and Co-based materials, the CCN3-PMS system has obvious advantages not only in the amount of catalyst, but also in the speed of degradation (Table S2). Therefore, the CCN3-PMS system can be promisingly used in the organic wastewater treatment. In the actual domestic filtrate wastewater (pre-treated) treatment (Figure S7 and Table S3), the CCN3-PMS system had about 38.7% removal rate of COD and 30.1% removal rate of ammonia nitrogen.

3.3. Reaction mechanism of the CCN-PMS system

To investigate the degradation mechanism of organic pollutants in the CCN-PMS system, the reactive oxygen species (ROS) in the system were confirmed by radical quenching experiments and EPR analysis. Previous studies reveal that $SO_4^{\bullet-}$, •OH, $\bullet O_2^-$ or $^1O_2$, or several of them were produced in catalytic activated PMS systems [38,39]. Here, methanol (MeOH) as $SO_4^{\bullet-}$ and •OH radical scavenger, *tert*-butanol (TBA) as •OH radical scavenger, p-benzoquinone (BQ) as $\bullet O_2^-$ radical scavenger, and 2,2,6,6-tetramethylpiperidine (TEMP) as $^1O_2$ non-radical scavenger were chosen to identify the critical oxidants in the TC degradation process [40]. After adding MeOH, the degradation efficiency of TC decreased significantly from 91.3% to 66.8% (Fig. 7a), whereas the oxidation performance of the system retained with the addition of TBA. Similar to TBA, BQ presented a negligible effect on the degradation of TC (Fig. 7b). These results prove that $SO_4^{\bullet-}$ was a more essential active agent than •OH and $\bullet O_2^-$ to oxidize TC in this system.

To further confirm whether radicals such as $SO_4^{\bullet-}$, •OH, and $\bullet O_2^-$ were generated during the reaction, EPR spectra were recorded in different scavenger systems. The radicals generated in the CCN3-PMS system were further monitored by coupling the EPR and dimethyl pyridine N-oxide (DMPO), which was used to capture $SO_4^{\bullet-}$ and •OH. The representative signals of DMPO-•OH and DMPO-$SO_4^{\bullet-}$ recorded during the experiments confirmed the existence of $SO_4^{\bullet-}$ and •OH (Fig. 7c). After adding excess methanol, the representative signal of $\bullet O_2^-$ can also be detected (Fig. 7d), but it showed negligible effect on the system through the above quenching experiments. To explore the formation process of $SO_4^{\bullet-}$ and •OH, the valence change of Co before and after the reaction was analyzed according to XPS. As shown in Figure S2b, the fitted peaks at 779.5 eV and 794.8 eV in the post-reaction Co 2p XPS spectrum were consistent with the signals of Co $2p_{3/2}$ and Co $2p_{1/2}$ of Co^{3+} [41]. During the changing of the valence state of Co, it is

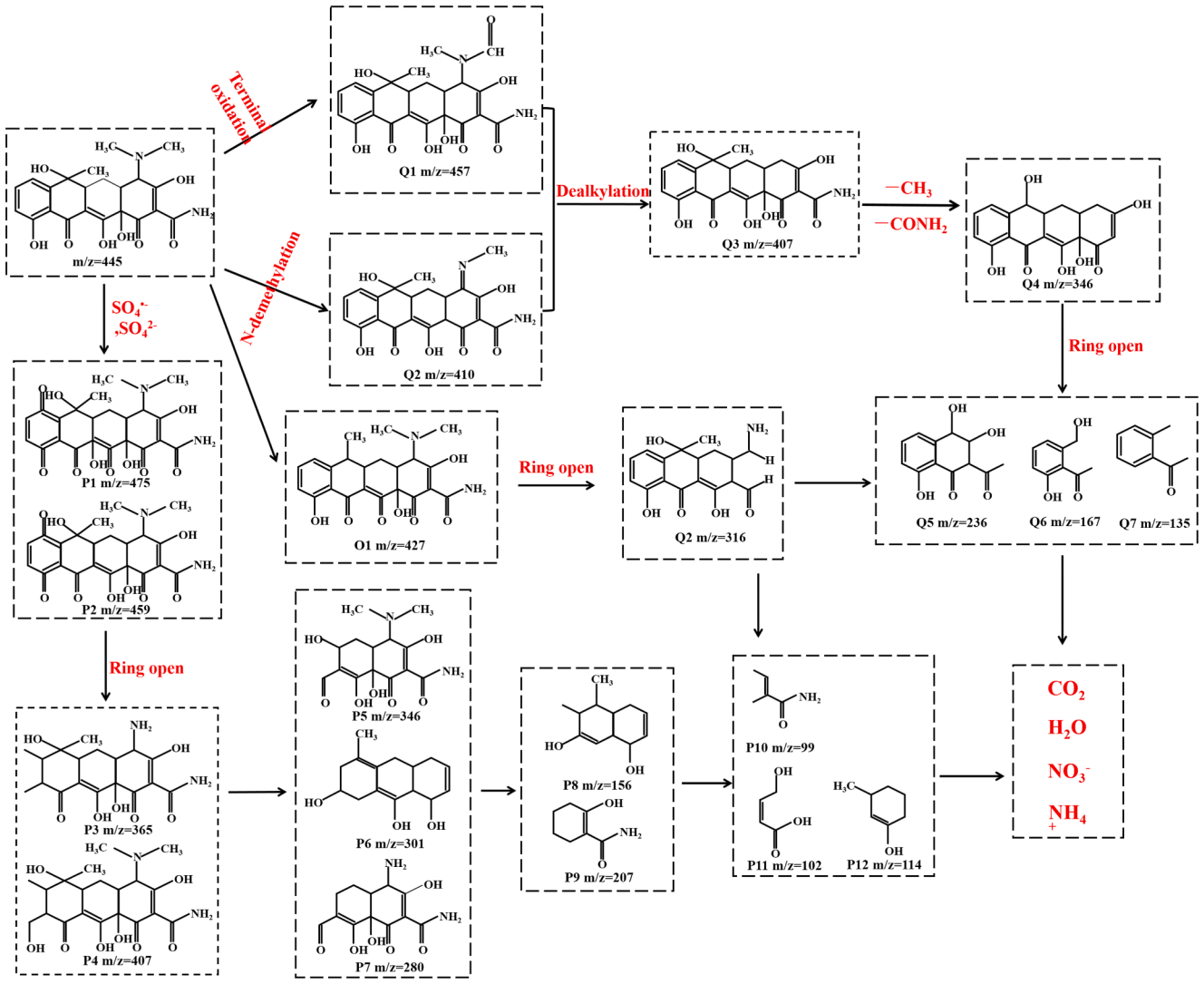

Fig. 8. Possible pathways for tetracycline in the CCN3-PMS system.

hypothesized that Co^{2+} first reacts with HSO_5^- to form Co^{3+}, which subsequently reacts with HSO_5^- to regenerate Co^{2+}, while Co accelerates the reaction from Co^{3+} to Co^{2+}. In the Co-mediated PMS activation system according to the equations (1), (2), (3) and (4), the active substances are $SO_4^{\bullet-}$ and •OH, where $SO_4^{\bullet-}$ is the dominant active substance [42]. However, more than 40% of the TC was degraded in this system even with the addition of excess methanol, and most of the $SO_4^{\bullet-}$ and •OH were quenched. This result indicates that both radical and non-radical reaction pathways existed in the CCN-PMS system.

$$Co^{2+}+HSO_5^-\rightarrow Co^{3+}+ SO_4^{\bullet-}+OH^- \quad (1)$$

$$Co^{3+}+HSO_5^-\rightarrow Co^{2+}+SO_5^{\bullet-}+H^+ \quad (2)$$

$$SO_4^{\cdot-}+OH^-\rightarrow SO_4^{2-}+\bullet OH \quad (3)$$

$$Co^{3+}+Co \rightarrow Co^{2+} \quad (4)$$

To reveal the active sites of the radical and non-radical pathways in the CCN3-PMS system, the performance of the NC-PMS system for degradation of TC was tested. The catalytic activity of NC was much lower than that of CCN3 (Fig. 7e). Radical quenching experiments with methanol showed that the activity of the CCN3-PMS system was also suppressed, which was similar to that of the NC-PMS system without methanol. However, the quenching effect of methanol on the NC-PMS system was more minor. This result indicates that the addition of the Co source generated more radicals ($SO_4^{\bullet-}$ and •OH), further confirming that the NC-PMS system relied on the non-radical pathways to degrade organic pollutants [43].

Non-radical pathways have been recognized in many catalytic PMS oxidations of organic pollutants. The formation of singly linear oxygen ($^1O_2$), mediating electron transfer pathways in non-homogeneous catalysts and direct oxidation pathways are typical mechanisms in non-radical catalytic PMS system [44]. In this experiment, the formation of $^1O_2$ was confirmed by quenching experiments with L-histidine or TEMP and EPR analysis. The degradation rate of TC decreased significantly with the addition of TEMP (Fig. 7b). Using Tetramethylpiperidone oxide (TMPO) as a spin trapping agent, the EPR spectra showed that the equal intensity for the TEMPO adduct triple peak signal was detectable (Fig. 7f), suggesting that $^1O_2$ was the potential active compound for degrading the pollutants. However, the electron transfer reaction can also produce the same EPR signal during an EPR analysis [45]. Hence, linear scanning voltammetry (LSV) and impedance testing (EIS) were performed to demonstrate whether direct electron transfer pathways exist on carbon-based materials to degrade TC [33]. Compared with CCN3, the current and impedance of CCN3 + PMS and CCN3 + PMS + TC systems did not change significantly (Fig. 7g-h), indicating that the existence of the electron transfer pathway of the catalyst was negligible during the activation of PMS by CCN3 catalyst. It is well known that PMS can be catalyzed by ketones to produce $^1O_2$, while the surface of CCN3

contains a large number of carbonyl groups [27]. This finding explains that $^1O_2$ was produced during the activation of PMS by the CCN3 catalyst in the CCN3-PMS system. In addition, the graphite N doping in the CCN3 will induce electron transfer from the adjacent C atom to the N atom. Thus, the C atoms adjacent to graphite N (carbon in the C═O group) react more easily with HSO_5^- in PMS and promote the production of $^1O_2$ [21]. The reaction equation (5) is as follows.

$$R\text{-}\overset{O}{\overset{\|}{C}}\text{-}R + HSO_5^- \longrightarrow {}^1O_2 + SO_4^{2-} + R\text{-}\overset{O}{\overset{\|}{C}}\text{-}R \quad (5)$$

Based on the above results, the basic process of the generation of radicals and the degradation of TC can be inferred in Fig. 7I. The mainly radicals were generated by the Co@CoO, while the mainly non-radicals were generated by the N-doped carbon nanotubes. The $^1O_2$ and $SO_4^{\bullet-}$ were responsible for the non-radical, the radical respectively in the CCN3-PMS system. The Co@CoO internal electron transfer accelerates the cycle of conversion between Co^{2+} and Co^{3+}.

3.4. Intermediate and degradation pathway of TC

As TC molecules have a variety of groups, their degradation products and pathways are rather complex [46]. According to the mass spectra (Figure S8), substances with different *m/z* values were detected, and four possible degradation pathways were inferred in combination with the different groups attacked by different ROS. Fig. 8 displays that the TC molecule was attacked by $SO_4^{\bullet-}$, •OH and $^1O_2$ and decomposed into lower molecular weight products. The main pathways of degradation were classified as terminal oxidation, N-dealkylation, demethylation and ring-opening [46]. Interestingly, different ways of opening rings during the process of degradation could be derived, probably due to the synergistic effect of radicals and non-radical [47]. In the presence of $SO_4^{\bullet-}$ and SO_4^{2-} [48], important the reactions of TC would occur in the following order: *i*) terminal oxidation to form P1 ($m/z = 475$) and P2($m/z = 459$); *ii*) ring opening to form P3 ($m/z = 365$) and P4 ($m/z = 407$); *iii*) decomposition to P5 ($m/z = 346$), P6 ($m/z = 301$) and P7 ($m/z = 280$); *iv*) conversion to P8 ($m/z = 156$) and P9 ($m/z = 207$); *iv*) further reaction to form P10 ($m/z = 99$), P11 ($m/z = 102$), and P12 ($m/z = 114$). In the other three degradation pathways, the order of occurrence would be: *i*) N-dealkylation and terminal oxidation to produce Q1 ($m/z = 457$) and Q2 ($m/z = 410$); *ii*) demethylation to produce Q3 ($m/z = 407$), and Q4 ($m/z = 346$) by the removal of CO-NH_2 groups; *iii*) ring-opening to produce Q5 ($m/z = 258$) Q6 ($m/z = 167$) and Q7 ($m/z = 135$); *i*) decomposition to O1 ($m/z = 427$), *ii*) ring opening to form O2, and decomposition to the smaller molecules. Based on the analysis of the results from LC-Q-TOF, it is inferred that the radicals were mainly responsible for the removal of side chain groups, while the non-radicals were more responsible for the ring-opening sites [49]. Then further, the action of both free radicals and non-free radicals together resulted in the TC mineralization to NH_4^+, NO_3^-,CO_2 and H_2O [8].

4. Conclusion

Co@CoO encapsulated with N-doped carbon nanotubes (CCN) was used for activating PMS to degrade pollutants for the first time. The optimized CCN-PMS system showed excellent purification performance for organic wastewater, with a degradation rate of over 92% in 30 min and the TOC removal rate of over 82% in 180 min, when dealing with 80 $mg{\cdot}L^{-1}$ TC (100 mL) pollutant. The N-doped carbon nanotubes can effectively encapsulate Co, which not only reduces the dissolution of Co and the secondary pollution to the environment, but also increases the stability of the catalyst and provides non-radical active sites. The CCN-PMS system was revealed to degrade pollutants through the coexistence of radicals and non-radicals. This work will deepen the understanding of the mechanism of PMS activation by carbon-based catalysts.

CRediT authorship contribution statement

Chuanyi Xu: Investigation, Writing – original draft. **Qingyou Liu:** Conceptualization, Writing – review & editing. **Meng Wei:** Validation. **Shihui Guo:** Investigation. **Yueping Fang:** Funding acquisition. **Zhuobiao Ni:** Writing – review & editing, Funding acquisition. **Xixian Yang:** Writing – review & editing. **Shengsen Zhang:** Supervision, Methodology, Writing – review & editing, Funding acquisition. **Rongliang Qiu:** Conceptualization, Writing – review & editing.

Declaration of Competing Interest

The authors declare that they have no known competing financial interests or personal relationships that could have appeared to influence the work reported in this paper.

Acknowledgements

This research was supported by the National Natural Science Foundation of China (22078118, 21972048, 42177208), Guangdong Provincial Science and Technology Project (2021B1212040008, 20210204), Key Realm Research and Development Program of Guangdong Province (2020B0202080001), and Natural Science Foundation of Guangdong Province, China (2019A1515011138).

Appendix A. Supplementary material

Supplementary data to this article can be found online at https://doi.org/10.1016/j.seppur.2022.121347.

References

[1] S. Xiang, H. Dong, Y. Li, J. Xiao, Q. Dong, X. Hou, D. Chu, A comparative study of activation of peroxymonosulfate and peroxydisulfate by greigite (Fe_3S_4) for the degradation of sulfamethazine in water, Sep. Purif. Technol. 290 (2022), 120873.
[2] M. Wang, Y. Cui, H. Cao, P. Wei, C. Chen, X. Li, J. Xu, G. Sheng, Activating peroxydisulfate with Co_3O_4/$NiCo_2O_4$ double-shelled nanocages to selectively degrade bisphenol A – A nonradical oxidation process, Appl. Catal. B: Environ. 282 (2021), 119585.
[3] J. Wang, H. B, M. Yang, R. Liu, C. Hu, H. Liu, J. Qu, Anaerobically-digested sludge disintegration by transition metal ions-activated peroxymonosulfate (PMS): comparison between Co^{2+}, Cu^{2+}, Fe^{2+} and Mn^{2+}, Sci Total Environ. 713 (2020), 136530.
[4] A. Fernandes, P. Makoś, G. Boczkaj, Treatment of bitumen post oxidative effluents by sulfate radicals based advanced oxidation processes (S-AOPs) under alkaline pH conditions, J. Clean. Prod. 195 (2018) 374–384.
[5] L. Liu, S. Lin, W. Zhang, U. Farooq, G. Shen, S. Hu, Kinetic and mechanistic investigations of the degradation of sulfachloropyridazine in heat-activated persulfate oxidation process, Chem. Eng. J. 346 (2018) 515–524.
[6] F. Moradian, B. Ramavandi, N. Jaafarzadeh, E. Kouhgardi, Effective treatment of high-salinity landfill leachate using ultraviolet/ultrasonication/peroxymonosulfate system, Waste Manage. 118 (2020) 591–599.
[7] K. Wang, S. Zhang, R. Wang, Y. Liu, G. Cao, X. Duan, S.-H. Ho, Rational design of Spirulina residue-derived graphene oxide as an efficient metal-free catalyst for sulfathiazole removal, Sep. Purif. Technol. 290 (2022), 120862.
[8] Q. Yi, J. Tan, W. Liu, H. Lu, M. Xing, J. Zhang, Peroxymonosulfate activation by three-dimensional cobalt hydroxide/graphene oxide hydrogel for wastewater treatment through an automated process, Chem. Eng. J. 400 (2020), 125965.
[9] S. Giannakis, K.-Y.-A. Lin, F. Ghanbari, A review of the recent advances on the treatment of industrial wastewaters by sulfate radical-based advanced oxidation processes (SR-AOPs), Chem. Eng. J. 406 (2021), 127083.
[10] H. Li, Z. Zhao, J. Qian, B. Pan, Are free radicals the primary reactive species in Co (II)-mediated activation of peroxymonosulfate? new evidence for the role of the Co (II)–peroxymonosulfate complex, Environ. Sci. Technol. 55 (9) (2021) 6397–6406.
[11] Z. Wu, Y. Wang, Z. Xiong, Z. Ao, S. Pu, G. Yao, B. Lai, Core-shell magnetic Fe_3O_4@Zn/Co-ZIFs to activate peroxymonosulfate for highly efficient degradation of carbamazepine, Appl. Catal. B: Environ. 277 (2020), 119136.
[12] X. Sun, D. Xu, P. Dai, X. Liu, F. Tan, Q. Guo, Efficient degradation of methyl orange in water via both radical and non-radical pathways using Fe-Co bimetal-doped MCM-41 as peroxymonosulfate activator, Chem. Eng. J. 402 (2020), 125881.
[13] J. Tan, C. Xu, X. Zhang, Y. Huang, MOFs-derived defect carbon encapsulated magnetic metallic Co nanoparticles capable of efficiently activating PMS to rapidly degrade dyes, Sep. Purif. Technol. 289 (2022), 120812.
[14] P.R. Shukla, S. Wang, H. Sun, H.M. Ang, M. Tadé, Activated carbon supported cobalt catalysts for advanced oxidation of organic contaminants in aqueous solution, Appl. Catal. B: Environ. 100 (3–4) (2010) 529–534.

[15] W. Tian, H. Zhang, Z. Qian, T. Ouyang, H. Sun, J. Qin, M.O. Tadé, S. Wang, Bread-making synthesis of hierarchically Co@C nanoarchitecture in heteroatom doped porous carbons for oxidative degradation of emerging contaminants, Appl. Catal. B: Environ. 225 (2018) 76–83.
[16] W. Ma, N. Wang, Y. Fan, T. Tong, X. Han, Y. Du, Non-radical-dominated catalytic degradation of bisphenol a by ZIF-67 derived nitrogen-doped carbon nanotubes frameworks in the presence of peroxymonosulfate, Chem. Eng. J. 336 (2018) 721–731.
[17] X. Duan, H. Sun, Z. Shao, S. Wang, Nonradical reactions in environmental remediation processes: uncertainty and challenges, Appl. Catal. B: Environ. 224 (2018) 973–982.
[18] Y. Yao, H. Chen, C. Lian, F. Wei, D. Zhang, G. Wu, B. Chen, S. Wang, Fe Co, Ni nanocrystals encapsulated in nitrogen-doped carbon nanotubes as Fenton-like catalysts for organic pollutant removal, J. Hazard. Mater. 314 (2016) 129–139.
[19] H. Sun, X. Peng, S. Zhang, S. Liu, Y. Xiong, S. Tian, J. Fang, Activation of peroxymonosulfate by nitrogen-functionalized sludge carbon for efficient degradation of organic pollutants in water, Bioresource Technol. 241 (2017) 244–251.
[20] H. Liu, P. Sun, M. Feng, H. Liu, S. Yang, L. Wang, Z. Wang, Nitrogen and sulfur co-doped CNT-COOH as an efficient metal-free catalyst for the degradation of UV filter BP-4 based on sulfate radicals, Appl. Catal. B: Environ. 187 (2016) 1–10.
[21] D. Ding, S. Yang, X. Qian, L. Chen, T. Cai, Nitrogen-doping positively whilst sulfur-doping negatively affect the catalytic activity of biochar for the degradation of organic contaminant, Appl. Catal. B: Environ. 263 (2020), 118348.
[22] C. Chen, C. Jiang, W. Cao, H. Zhou, Y. Wang, Insight into the difference in activation of peroxymonosulfate with nitrogen-doped and non-doped carbon catalysts to degrade bisphenol A, J. Environ. Eng. 9 (4) (2021) 105492.
[23] G. Yang, Y. Li, S. Yang, J. Liao, X. Cai, Q. Gao, Y. Fang, F. Peng, S. Zhang, Surface oxidized nano-cobalt wrapped by nitrogen-doped carbon nanotubes for efficient purification of organic wastewater, Sep. Purif. Technol. 259 (2021), 118098.
[24] W. Hu, J. Tan, G. Pan, J. Chen, Y. Chen, Y. Xie, Y. Wang, Y. Zhang, Direct conversion of wet sewage sludge to carbon catalyst for sulfamethoxazole degradation through peroxymonosulfate activation, Sci Total Environ. 728 (2020), 138853.
[25] D. Ouyang, Y. Chen, J. Yan, L. Qian, L. Han, M. Chen, Activation mechanism of peroxymonosulfate by biochar for catalytic degradation of 1,4-dioxane: Important role of biochar defect structures, Chem. Eng. J. 370 (2019) 614–624.
[26] C.F. Li, J.W. Zhao, L.j. Xie, J.Q. Wu, G.R. Li, Water adsorption and dissociation promoted by Co*-/N-C*-biactive sites of metallic Co/N-doped carbon hybrids for efficient hydrogen evolution, Appl. Catal. B: Environ. 282 (2021), 119463.
[27] Y. Wang, Y. Song, N. Li, W. Liu, B. Yan, Y. Yu, L. Liang, G. Chen, L.a. Hou, S. Wang, Tunable active sites on biogas digestate derived biochar for sulfanilamide degradation by peroxymonosulfate activation, J. Hazard. Mater. 421 (2022), 126794.
[28] H. Fan, L.u. Qiu, A. Fedorov, M.-G. Willinger, F. Ding, X. Huang, Dynamic state and active structure of Ni–Co catalyst in carbon nanofiber growth revealed by in situ transmission electron microscopy, ACS Nano. 15 (11) (2021) 17895–17906.
[29] Y. Wang, L.u. Qiu, L. Zhang, D.-M. Tang, R. Ma, Y. Wang, B. Zhang, F. Ding, C. Liu, H.-M. Cheng, Precise identification of the active phase of cobalt catalyst for carbon nanotube growth by in situ transmission electron microscopy, ACS Nano. 14 (12) (2020) 16823–16831.
[30] X. Zhao, Q.-D. An, Z.-Y. Xiao, S.-R. Zhai, Z. Shi, Seaweed-derived multifunctional nitrogen/cobalt-codoped carbonaceous beads for relatively high-efficient peroxymonosulfate activation for organic pollutants degradation, Chem. Eng. J. 353 (2018) 746–759.
[31] C. Wang, J. Yin, R. Wang, T. Jiao, H. Huang, J. Zhou, L. Zhang, Q. Peng, Facile Preparation of Self-assembled polydopamine-modified electrospun fibers for highly effective removal of organic dyes, Nanomaterials. 9 (2019) 116.
[32] C. Chen, L. Liu, J. Guo, L. Zhou, Y. Lan, Sulfur-doped copper-cobalt bimetallic oxides with abundant Cu(I): a novel peroxymonosulfate activator for chloramphenicol degradation, Chem. Eng. J. 361 (2019) 1304–1316.
[33] T. Yang, S. Fan, Y. Li, Q. Zhou, Fe-N/C single-atom catalysts with high density of Fe-Nx sites toward peroxymonosulfate activation for high-efficient oxidation of bisphenol a: electron-transfer mechanism, Chem. Eng. J. 419 (2021), 129590.
[34] X. Duan, H. Sun, Y. Wang, J. Kang, S. Wang, N-doping-induced nonradical reaction on single-walled carbon nanotubes for catalytic phenol oxidation, ACS Catal. 5 (2) (2015) 553–559.
[35] Y. Ji, C. Dong, D. Kong, J. Lu, New insights into atrazine degradation by cobalt catalyzed peroxymonosulfate oxidation: kinetics, reaction products and transformation mechanisms, J. Hazard. Mater. 285 (2015) 491–500.
[36] M. Golshan, B. Kakavandi, M. Ahmadi, M. Azizi, Photocatalytic activation of peroxymonosulfate by TiO_2 anchored on cupper ferrite (TiO_2@$CuFe_2O_4$) into 2,4-D degradation: process feasibility, mechanism and pathway, J. Hazard. Mater. 359 (2018) 325–337.
[37] S. Wu, H. He, X. Li, C. Yang, G. Zeng, B. Wu, S. He, L. Lu, Insights into atrazine degradation by persulfate activation using composite of nanoscale zero-valent iron and graphene: performances and mechanisms, Chem. Eng. J. 341 (2018) 126–136.
[38] Z. Wang, Y. Han, W. Fan, Y. Wang, L. Huang, Shell-core MnO_2/carbon@carbon nanotubes synthesized by a facile one-pot method for peroxymonosulfate oxidation of tetracycline, Sep. Purif. Technol. 278 (2021), 119558.
[39] Y. Xu, E. Hu, D. Xu, Q. Guo, Activation of peroxymonosulfate by bimetallic CoMn oxides loaded on coal fly ash-derived SBA-15 for efficient degradation of Rhodamine B, Sep. Purif. Technol. 274 (2021), 119081.
[40] C. Xu, G. Yang, J. Li, S. Zhang, Y. Fang, F. Peng, S. Zhang, R. Qiu, Efficient purification of tetracycline wastewater by activated persulfate with heterogeneous Co-V bimetallic oxides, J. Colloid. Interf. Sci. 619 (2022) 188–197.
[41] Z. Zhao, Q. Sha, K. Ma, Y. Lu, Liquid-to-gas transition derived cobalt-based nitrogen-doped carbon nanosheets with hierarchically porous for oxygen reduction reaction, Appl. Surf. Sci. 509 (2020), 145365.
[42] C. Liu, S. Liu, L. Liu, X. Tian, L. Liu, Y. Xia, X. Liang, Y. Wang, Z. Song, Y. Zhang, R. Li, Y. Liu, F. Qi, W. Chu, D.C.W. Tsang, B. Xu, H. Wang, A. Ikhlaq, Novel carbon based Fe-Co oxides derived from Prussian blue analogues activating peroxymonosulfate: refractory drugs degradation without metal leaching, Chem. Eng. J. 379 (2020), 122274.
[43] H. Ma, G. Wang, Z. Miao, X. Dong, X. Zhang, Integration of membrane filtration and peroxymonosulfate activation on CNT@nitrogen doped carbon/Al_2O_3 membrane for enhanced water treatment: insight into the synergistic mechanism, Sep. Purif. Technol. 252 (2020) 117479.
[44] H. Xu, N. Jiang, D. Wang, L. Wang, Y. Song, Z. Chen, J. Ma, T. Zhang, Improving PMS oxidation of organic pollutants by single cobalt atom catalyst through hybrid radical and non-radical pathways, Appl. Catal. B: Environ. 263 (2020), 118350.
[45] G. Nardi, I. Manet, S. Monti, M.A. Miranda, V. Lhiaubet-Vallet, Scope and limitations of the TEMPO/EPR method for singlet oxygen detection: the misleading role of electron transfer, Free. Radical. Bio. Med. 77 (2014) 64–70.
[46] Y. Chen, R. Yin, L. Zeng, W. Guo, M. Zhu, Insight into the effects of hydroxyl groups on the rates and pathways of tetracycline antibiotics degradation in the carbon black activated peroxydisulfate oxidation process, J. Hazard. Mater. 412 (2021), 125256.
[47] X. Li, T. Hou, L. Yan, L. Shan, X. Meng, Y. Zhao, Efficient degradation of tetracycline by CoFeLa-layered double hydroxides catalyzed peroxymonosulfate: synergistic effect of radical and nonradical pathways, J. Hazard. Mater. 398 (2020), 122884.
[48] Y. Ji, Y. Shi, W. Dong, X. Wen, M. Jiang, J. Lu, Thermo-activated persulfate oxidation system for tetracycline antibiotics degradation in aqueous solution, Chem. Eng. J. 298 (2016) 225–233.
[49] Y. Zhang, J. Zhou, X. Chen, L. Wang, W. Cai, Coupling of heterogeneous advanced oxidation processes and photocatalysis in efficient degradation of tetracycline hydrochloride by Fe-based MOFs: Synergistic effect and degradation pathway, Chem. Eng. J. 369 (2019) 745–757.